Landing of an Airliner Using Image Based Visual Servoing

Gibert Victor * **Puyou Guilhem** **

* *Airbus Operations S A S, 316 route de Bayonne 31060 Toulouse France (e-mail: victor.gibert@airbus.com).*
** *Airbus Operations S A S, 316 route de Bayonne 31060 Toulouse France (e-mail: guilhem.puyou@airbus.com).*

Abstract: In this paper, an image-based visual servoing scheme is presented in order to control a transport aircraft in final approach phase by overcoming the need for external information (e.g. ILS or GPS systems) and runway knowledge. Based on three decoupled visual features and inertial data, the guidance scheme is designed and validated on a simplified model and tested on a realistic nonlinear simulator. Finally simulation results are presented in order to validate the choice of the visual features and the guidance laws to land the aircraft.

Keywords: Autonomous Landing, Aircraft Control, Visual Servoing, Visual Features

1. INTRODUCTION

Up to now, automatic landing of a transport aircraft usually requires an equipped airport. ILS (Instrument Landing System) is the most common used technology and it allows aircraft to land without pilot action (expect monitoring). Thanks to the ILS signals, on-board computers are able to deliver deviation to the reference axis (LOC and Glide Slope) to the guidance laws. However this equipment is expensive and thus not available at every airport. In the frame of the future aircraft generation, Airbus wishes to develop a capacity of automatic landing everywhere (unequipped or unknown airport) and anytime (very low propability of failure).

Current technology for localization like GPS, IRS (Inertial Reference System) or VOR/DME [1] is sufficiently accurate to place the aircraft under acceptable conditions close to the landing area but not precise enough to land on a runway. To do so a GPS augmentation system is required. It may be a local augmentation (ex: GBAS using ground stations) or regional (SBAS using satellite network like WAAS or EGNOS). GBAS is located on the airport, which is not compatible with our desire to land everywhere. SBAS could meet the everywhere requirement (Hughes, October 2012), however forecasted availability rate (99.95%) is not enough. Moreover, it requires knowledge of the runway so other constraints appear (database availability, integrity, completness issues).

To cope with these issues (availability of an accurate absolute position or database) and extend automatic landing coverage, the use of a camera as an additional source of information is going to be investigated. In the last ten years camera technology has made a technological leap so that equiping every aircraft seems to be easy and cheep. In this paper, it is assumed that visibility is good enough so visible frequency range is sufficient. However for an extension of the operational domain, those results could be generalized to other kinds of images: Infra Red or millimeter-wave camera.

There are two main ways of using vision in the control scheme especially for landing. One is PBVS (Pose Based Visual Servoing), the other is IBVS (Image Based Visual Servoing). PBVS is based on visual information to estimate the 3D pose (position and attitude) of the system. This estimation can be done by knowing the target caracteristics, by stereo-vision or by knowing the motion between two images. In IBVS, visual features are directly specified from the image frame of the camera. A lot of work has been done especially using interaction matrix which links visual features to camera velocity (Silveira et al., 2003)(Azinheira and Rives, 2008)(Le Bras et al., 2009)(Goncalves et al., 2010).

Among these strategies, IBVS seems to be more independent from runway knowledge because features can be expressed in relative terms in the image frame. That's why our study focuses on IBVS. The aim of this article is to benchmark existing approaches. (Bourquardez and Chaumette, 2007a) and (Coutard et al., 2011) works have been selected because they seem to have good enough results on the same application. After applying them to the same model, a new set of features is proposed as an enhancement over the previous strategies. The main selection criterion will be the performance compared to the baseline on the reference scenario, the decoupling between axes and the independence from the runway knowledge.

All visual servoing strategies rely on runway features detection. The used algorithms are not discussed in this paper. Moreover, vision is used to cope with relative position information, however availability of IRS information can be always assumed.

The paper is organized as follows. The first section will detail the sizing scenario, the assumptions and the requirements. Then the models used for both design and validation will be explained. In the next section control

[1] VHF Omnidirectional Range/Distance Measuring Equipment

strategies will be presented and applied on the benchmark model. After short critical reviews of the results, this paper will conclude on the submitted visual servoing strategy and will present the research axis to be investigated in the future

2. APPLICATION CONTEXT

2.1 Scenario and requirements

The covered scenarios begin at Δ_{X_0}=5000m with a maximum of Δ_{Y_0}= ±400m, Δ_{Z_0}= ±50m, Δ_{ρ_0}=±30° and Δ_{γ_0}=±4° (see Fig. 1). For this first study, wind perturbations are not considered.

Independence from runway data is important in order to land everywhere. Therefore the main constraint is to design a guidance law that doesn't use any position information, nor runway size knowledge. However, it is assumed that additional information is available: inertial measurements and air data give us the aircraft attitude, image processing gives us information in the image frame (runway lines and threshold) and the camera characteristics are known.

2.2 Baseline solution : LOC/GS guidance laws

Nowadays, automatic approach and landing (before flare and alignment) is based on deviations (Δ_Y and Δ_Z) provided by the ILS (see Fig. 1). This information is used by two guidance loops called LOC and Glide Slope (GS) to compute control loops inputs (roll rate angle $\dot{\phi}_c$ and vertical load factor N_{Z_c}). Fig. 2 resumes the global scheme where the navigation sensor block is composed of ILS sensors.

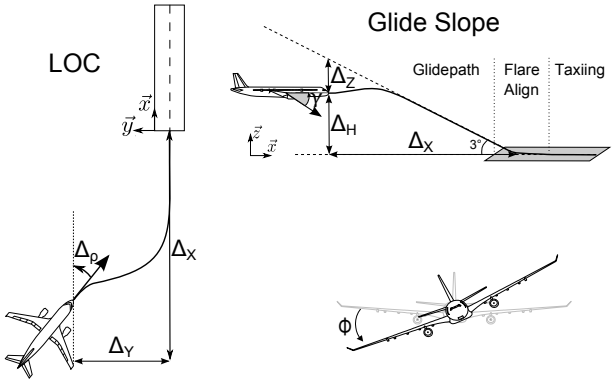

Fig. 1. Frames and Notations in ILS Final Approach

In final approach, the actual guidance loops can be simplified by the two following equations: (1) for the lateral, (2) for the vertical

$$\dot{\phi}_c = K_1\Delta_Y + K_2\Delta_\rho + K_3\phi + K_4\dot{\phi} \quad (1)$$

$$N_{Z_c} = K_5\Delta_Z + K_6\dot{\Delta}_Z \quad (2)$$

3. MODEL

The global simulation model for visual servoing is composed of two blocks of laws (guidance and control), aircraft dynamics and navigation sensors (see Fig. 2). In visual

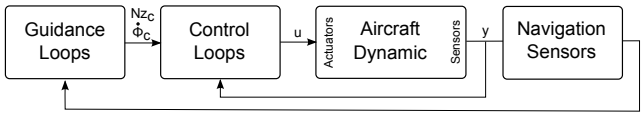

Fig. 2. Global Scheme for Guidance and Control

servoing, the navigation sensor block is composed of a camera with image processing algorithms.

In this paper, two variants of this global scheme are used. First, a simplified simulation model for the aircraft dynamics and control loops in order to design and validate the choice of visual features and the guidance loops. Then, the validated design is implemented on a simulator with certified non-linear aircraft dynamics and control loops. In these two variants, the navigation sensors block is composed of a perfect image processing.

3.1 Simplified model for control loops and aircraft

For the first design and validation study, each block of the global scheme (see Fig. 2) can be simplified by a new model. Control objectives are roll rate $\dot{\phi}_c$ and vertical load factor N_{Z_c}. It is assumed that the control loops and the aircraft short term dynamics (aerodynamic behavior) can be modeled by simple first-order transfer function that corresponds to the targeted closed loop dynamic (3) with τ=1.5s. In final approach, auto-throttle is engaged so that constant speed is assumed. Then a simplified aircraft kinematic model is included (4) [2]. Finally, positions are computed ($\Delta_X, \Delta_Y, \Delta_H$) assuming relations (5)(6)(7).

$$\frac{Nz}{Nz_c} = \frac{1}{1+\tau s} \; and \; \frac{\dot{\phi}}{\dot{\phi}_c} = \frac{1}{1+\tau s} \quad (3)$$

$$\gamma = \frac{g}{V}\int Nz \; and \; \psi = \frac{g}{V}\int \tan\phi \quad (4)$$

$$\dot{X} = V\cos\psi\cos\gamma \quad (5)$$

$$\dot{Y} = V\sin\psi\cos\gamma \quad (6)$$

$$\dot{H} = V\cos\psi\sin\gamma \quad (7)$$

3.2 Simplified Camera and Image processing model

In order to design the guidance loops, a perfect camera and image processing models are used. The image and the desired features are built from the aircraft pose by using the pinhole camera model based on perspective projection (see Fig. 3).

This camera model links the coordinates of a 3D point with its coordinates in pixel in the image (8).

$$P_c = \begin{bmatrix} {}^cR_o & {}^ct_o \\ 0 & 1 \end{bmatrix} P_o \quad (8)$$

Where ${}^cR_o$ and ${}^ct_o$ are the matrices of rotation and translation from the ground frame F_0 to the aircraft frame F_c. P_0= $(X_0, Y_0, Z_0, 1)_{F_0}$ and P_c= $(X_c, Y_c, Z_c, 1)_{F_c}$.

The next step is to derive the coordinates of the point P in the image plane P_π. Coordinates of the point in the image p=$(x_p, y_p, f)_{F_c}$ are obtained with (9) where f is the focal length.

[2] ψ is the heading of the aircraft. In our case, the runway heading is consider equal to zero so $\psi = \Delta_\rho$

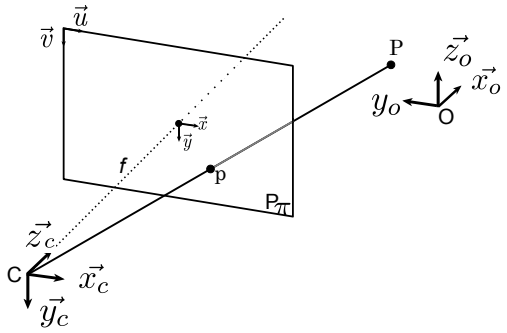

Fig. 3. Perspective Projection

$$x_p = f\frac{X_c}{Z_c} \text{ and } y_p = f\frac{Y_c}{Z_c} \tag{9}$$

Finally, the point is expressed into pixel coordinate which are usually expressed from the top left edge ($\boldsymbol{u}$,$\boldsymbol{v}$) taking into account the size of pixels.

In this paper, the perfect image processing model uses this method to build the four corners of the runway. Then from the corners coordinates in the image frame, visuals features are extracted. We consider the sampling period between image processing and controler equal which is not always true. It depends on image processing accuracy and quality.

Our system is supposed to have only one camera so we are not able to estimate the depth Z_c. This strong constraint led us to use IBVS which is not interested in the estimation of the aircraft pose.

4. VISUAL SERVOING

The most promising and recent approaches to land an aircraft using IBVS have been proposed by (Bourquardez and Chaumette, 2007a) and (Coutard et al., 2011). The current paper studies these approaches and proposes a new set of visual features. First of all, this paper focuses on the lateral solution of (Bourquardez and Chaumette, 2007a). Then better results are obtained with (Coutard et al., 2011) strategy. Finally, a new set of visual features is proposed in order to make visual features more decoupled.

4.1 Baseline guidance law

To design guidance laws, the model is linearized around a position close to the runway axis (Δ_Y=20m) and on the glide slope (Δ_Z=0m). Then an eigenstructure assignment method is applied on the output vector (see Magni (2002)).

For both longitudinal and lateral guidance laws (cf (1) and (2)), a dominant second order dynamic is desired with $t_{r_{5\%}}$=20s and very little overshoot (for lateral and longitudinal motion). By taking ξ=0.99 and ω_0=0.25, the desired eigenvalues are : $\lambda_{1,2}$=-0.2475±i0.0353.

For the lateral baseline solution, four desired eigenvalues can be selected. Two additional eigenvalues twice faster are chosen :$\lambda_{3,4} = -0.4950 \pm i0.0353$.

The guidance laws gains become :

$$K_{1,2,3,4} = [0.14, 2.01, -1.20, -1.23] \tag{10}$$

$$K_{5,6} = [-0.0016, -0.0225] \tag{11}$$

So as to validate the design and highlight the baseline controller performance, lateral and longitudinal motions are simulated separately and then the two motions are coupled. The results obtained (by the baseline) are presented (with dashed line) in Fig. 5, 7, 8, 9, 11, 12 and 16 to be compared to the visual servoing solutions.

4.2 Review of previous IBVS approaches

In (Bourquardez and Chaumette, 2007a) the following features are used : the center line of the runway (θ_C and ρ_C), the edges of the runway, right (θ_R and ρ_R) and left (θ_L and ρ_L) and the coordinates of the vanishing point f=(x_f, y_f) in the camera frame (see Fig. 4).

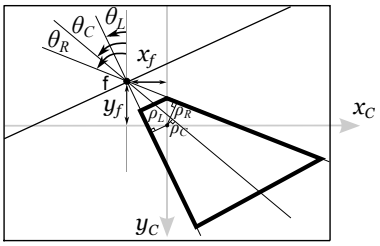

Fig. 4. Bourquardez Visual Features

The lateral guidance law uses a combination of them (12). To be consistent with the baseline, the structure has been slightly modified by adding a $\dot{\phi}$ term:

$$\dot{\phi_c} = K_1 \frac{H}{\cos^2\theta_L + \cos^2\theta_R - 2}(\theta_L + \theta_R - 2\theta_C) + K_2 x_f + K_3 \dot{x_f} + K_4 \dot{\phi} \tag{12}$$

When applied to the benchmark with the same eigenstructure assignment strategy that in subsection 4.1, the guidance laws gains become :

$$K_{1,2,3,4} = [0.22, 110.89, 405.9, -1.23] \tag{13}$$

Fig. 5 presents two different starting position (Δ_{Y_0}=20m or Δ_{Y_0}=100m). Results are good (i.e. close to the baseline) when the aircraft is close to the desired position but guidance laws are not performing in an appropriate manner when the position is far from the landing axis. Indeed, the aircraft doesn't land on the runway. To cope with that issue a reference trajectory strategy has been proposed in (Bourquardez and Chaumette, 2007b), however the generation of it assume that initial position is known (that is out of our assumptions). By the way, (12) shows that runway dimension is already used in the control law itself (13), through the parameter $H = \frac{L}{2\tan(\frac{\theta_L - \theta_R}{2})}$.

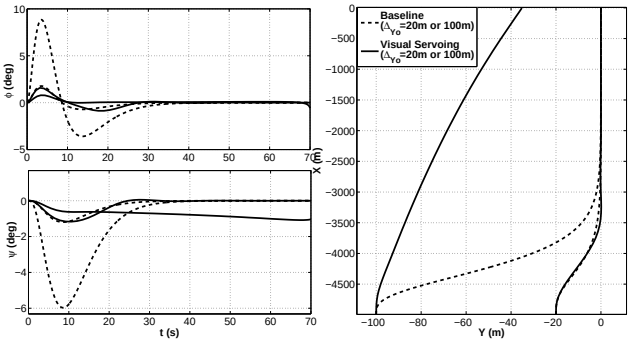

Fig. 5. Bourquardez Lateral Results (Δ_{Y_0}=20m or 100m)

(Coutard et al., 2011)'s strategy is based on other visual features: the center line (θ_R), the horizontal coordinate of

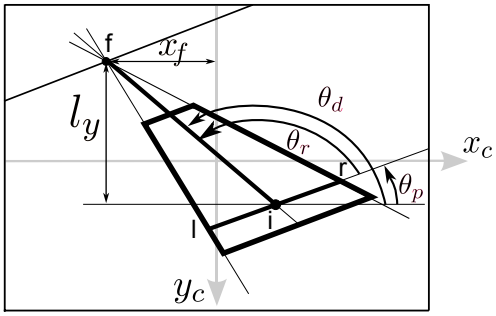

Fig. 6. Coutard Visual Features

the vanishing point (x_f) and the height (l_y) between the vanishing point and the impact point (see Fig. 6).

When applied to the benchmark, the new guidance loops are:

$$\dot{\phi_c} = K_1\theta_r + K_2 x_f + K_3\phi + K_4\dot{\phi} \quad (14)$$

$$N_{Z_c} = K_5 l_y + K_6 \dot{l_y} \quad (15)$$

The guidance laws gains become:

$$K_{1,2,3,4} = [35.6, 114.9, -1.8, -1.2] \quad (16)$$

$$K_{5,6} = [-8.2, -112.7] \quad (17)$$

The results are better (close to the baseline) even when the aircraft is far from the desired position (see Fig. 7).

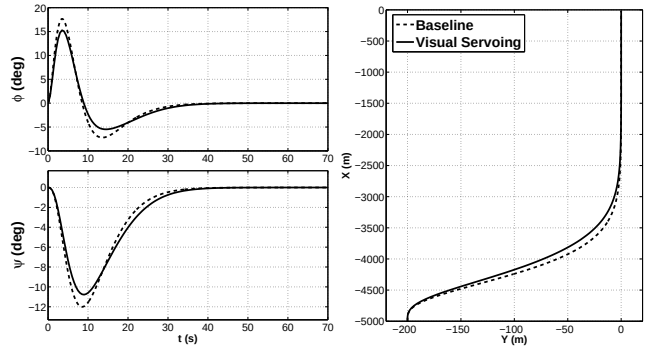

Fig. 7. Coutard Lateral Results (Δ_{Y_0}=200m)

When studying the worst case lateral initial position (Δ_Y=400m) within the defined scenario envelope, a difference appears between the reference (dashed line) and visual servoing (solid line) on the lateral motion (see Fig. 8). Even if the aircraft succeeds to land on the runway, results show that the system presents non-linearities (cf section 4.3) that need to be taken into account.

When the simulation couples lateral and longitudinal motions (see Fig. 9), results show influences between these two motions. Lateral behaviour presents a slight overshoot but seems totally acceptable compared with the baseline solution. Nevertheless, the longitudinal motion presents an abnormal behaviour in the 500 first meters. Indeed, the aircraft starts above the GS signal but the guidance loops make it climb instead of going down to capture the glide slope. This behaviour is due to a strong impact of roll angle ϕ and heading difference Δ_ρ on the l_y value.

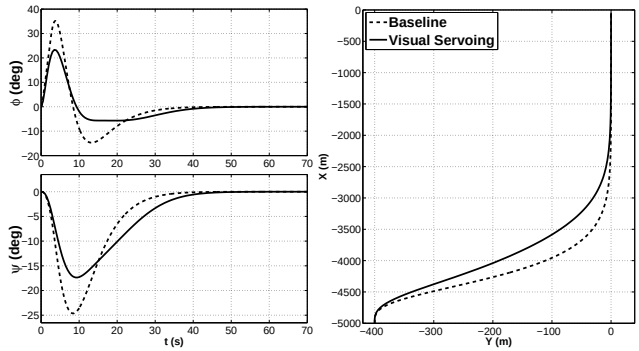

Fig. 8. Coutard Lateral Results (Δ_{Y_0}=400m)

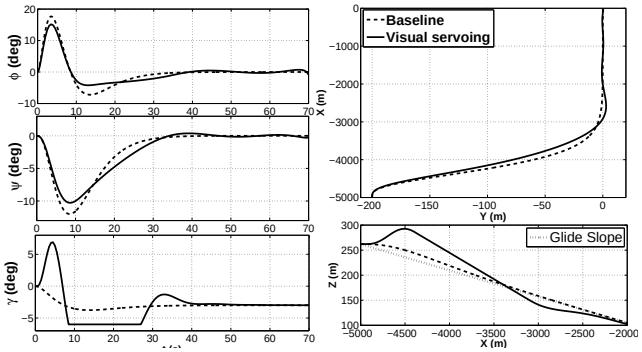

Fig. 9. Coutard Lateral and Longitudinal Results

4.3 Analysis of NL effects on simplified simulation loops

Although a simplified aircraft and control model is used, it is representative of the main non-linearities faced by the guidance loops. As a matter of fact, aerodynamic non-linearities are mastered by the control loops. This section studies the main non-linear effects on visual features with respect to the aircraft pose.

Relationships between Courtard's visual features and the pose parameters (Δ_X,Δ_Y,Δ_H,ϕ,θ and Δ_ρ) are the followings:

$$x_F = f(\frac{\cos\phi}{\cos\theta}\tan\Delta_\rho + \sin\phi\tan\theta) \quad (18)$$

$$\theta_R = atan(\frac{\cos\phi\cos\theta\Delta_Y - (\sin\phi\cos\Delta_\rho - \cos\phi\sin\Delta_\rho\sin\theta)\Delta_H}{\sin\phi\cos\theta\Delta_Y + (\cos\phi\cos\Delta_\rho - \sin\phi\sin\Delta_\rho\sin\theta)\Delta_H}) + \frac{\pi}{2} - \phi \quad (19)$$

$$l_y = f\frac{-\sin\phi\cos\Delta_\rho\Delta_Y + (\sin\phi\sin\Delta_\rho\sin\theta - \cos\phi\cos\Delta_\rho)\Delta_H}{\cos^2\Delta_\rho\cos^2\theta\Delta_X - \cos\Delta_\rho\sin\Delta_\rho\cos^2\theta\Delta_Y + \cos\Delta_\rho\cos\theta\sin\theta\Delta_H} \quad (20)$$

To understand the impact of the aircraft pose on the visual features, the baseline solution is played with Δ_{X_0}=5000m, Δ_{Y_0}=400m and Δ_{Z_0}= 0m (see Fig. 9) and plot visual features behaviour.

Parameter x_F.
Equation (18) states that x_F could be approximated by $f\tan\Delta_\rho$ but is influenced by ϕ. However Fig. 14 shows that this influence is minor.

Parameter θ_R.
Fig. 13 shows the difference between the values of θ_r obtained with two different initial positions (Δ_Y=200m and Δ_Y=400m) played by the baseline. It shows that θ_R is not proportional to Δ_Y with a fixed ratio. This effect is due to the "atan" function contained in the θ_R equation

(19). Fig. 13 also shows that the θ_R relationship can be simplified :

$$\theta_R \simeq atan(\frac{\Delta_Y}{\Delta_H}) \quad (21)$$

By looking the equation (21), we understand why coupling lateral and longitudinal motion introduces a different behaviour in Fig. 9. Δ_H has a strong effect, which is problematic because for a starting point closer to the runway (e.g. Δ_X=3000m), Δ_H will be smaller and the same guidance laws will not manage to land the aircraft on runway.

Parameter l_y.
The last visual feature (l_y) is used for vertical motion control but equation (20) highlights it is strongly linked to the lateral behaviour. Fig. 15 shows that during the first seconds of the simulation, l_y is negative whereas it should be positive because the aircraft is above the glide slope. During these first seconds, the value of ϕ is significant and the behaviour of l_y becomes false.

4.4 A new set of visual features

(Coutard et al., 2011) 's visual features seem limited. In order to make visual features more independent of different effects, a new set of visual features is proposed to avoid the previous problem and improve the global performance. To reduce the effect of the roll angle (ϕ) on l_y, the distance (d_y) is taken between the impact point and the horizon instead of the height of the vanishing point in relation to the impact point [3]. To reduce the effect of the roll angle (ϕ) on x_F, $\tan^{-1} d_F$ is taken instead of x_F. Equation (19) shows an influence of the *atan* function so $\tan\theta_R$ is simply taken instead of θ_R. However we don't manage to cope with Δ_Z influence for the moment.

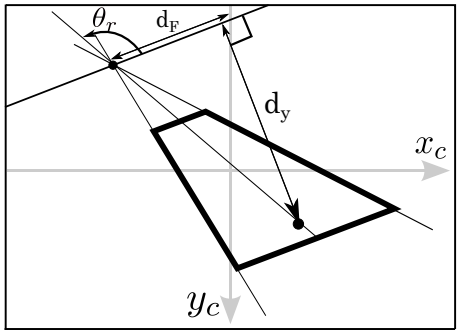

Fig. 10. New Set of Visual Features

Equation (22)(23) present relationships between visual features and aircraft pose.

$$d_F = \frac{x_F}{\cos\phi} = f(\frac{\tan\Delta_\rho}{\cos\theta} + \tan\phi\tan\theta) \quad (22)$$

$$d_y = f|\frac{\Delta_H}{\cos\Delta_\rho\cos^2\theta\Delta_X - \sin\Delta_\rho\cos^2\theta\Delta_Y + \cos\theta\sin\theta\Delta_H}| \quad (23)$$

With the new set of visual features, the guidance laws are decoupled as follows:

$$\dot{\phi_c} = K_1\tan\theta_r + K_2\tan^{-1} d_F + K_3\phi + K_4\dot{\phi} \quad (24)$$

$$N_{Z_c} = K_5\,\mathrm{d}_y + K_6\dot{d_y} \quad (25)$$

[3] We assume to know angles of the aircraft so we can build the theoretical horizon line in order to compute d_y and $\tan^{-1} d_F$. (see Fig. 10)

The guidance laws gains become:

$$K_{1,2,3,4} = [35.34, 114.92, -1.20, -1.23] \quad (26)$$

$$K_{5,6} = [-8.2, -112.7] \quad (27)$$

Lateral results with this new set of visual features (see Fig. 11) are very close to the baseline. A non-linearity influence has been removed.

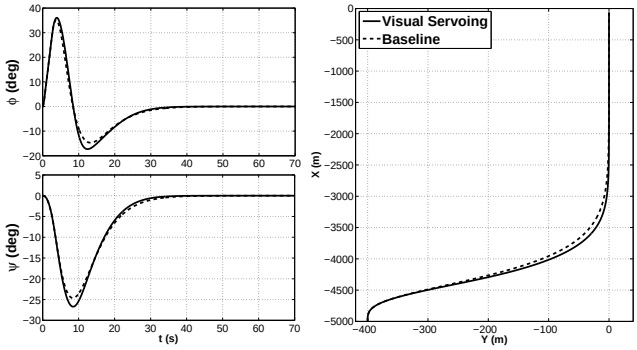

Fig. 11. New Set - Lateral Results (Δ_{Y_0}=400m)

Introducing axes coupling (see Fig. 12), lateral results are closed to the baseline even if a slight overshoot still appears. Longitudinal results show that the capture is done from the beginning so the longitudinal previous problem is avoided.

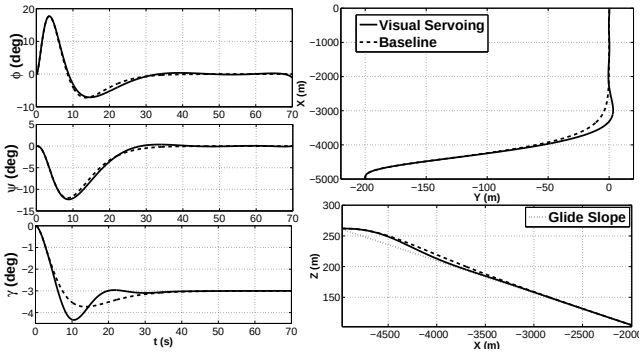

Fig. 12. New Set - Lateral and Longitudinal Results

A study of visual features has been done to understand the non-linearities influences and differences between visuals features. The new visual feature ($\tan\theta_R$) is linked with better fidelity to Δ_Y (see Fig. 13).

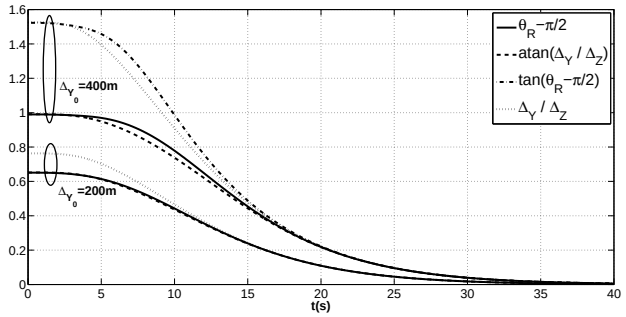

Fig. 13. θ_R, $\tan\theta_R$ and $\frac{\Delta_Y}{\Delta_Z}$ behaviours along the baseline

Looking at x_F and $\tan^{-1} d_F$ visual features (see Fig. 14), underlines that the relationship with Δ_ρ is important.

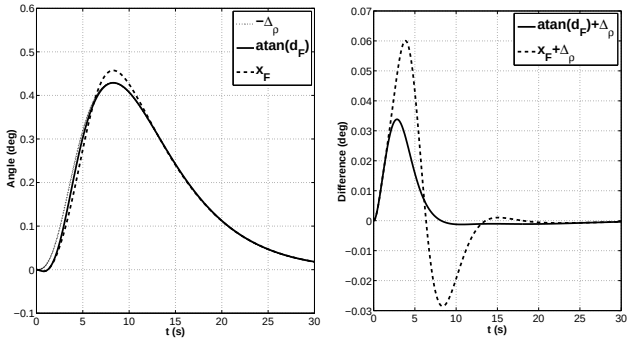

Fig. 14. x_F, $\tan^{-1} d_F$ and Δ_ρ behaviours along the baseline

It also point out that $\tan^{-1} d_F$ is closer to Δ_ρ than x_F because d_F is less influenced by ϕ.

Longitudinal visual features (l_y and d_y) present a important difference. Indeed, Fig. 15 explains why Coutard's solution has a missed dynamic response on the longitudinal axis (ϕ impact a lot l_y). It also shows a small lateral influences on d_y even if it is more representative of Δ_Z.

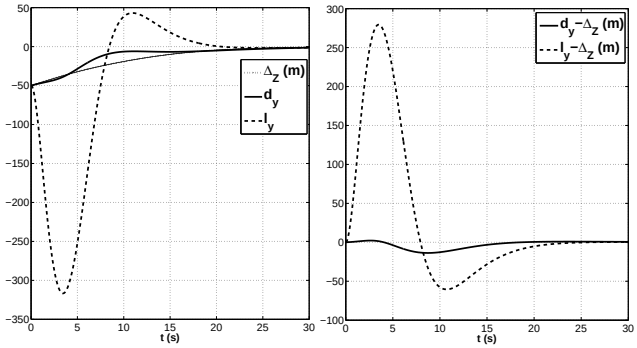

Fig. 15. l_y, d_y and Δ_Z behaviours along the baseline

4.5 Deeper validation using the full NL simulation loop

After the first validation step using a simplified aircraft model, the same guidance laws are implemented on the certified aircraft simulator. Results (see Fig. 16) show a good behaviour (compared to the baseline) of the aircraft with these guidance loops. The response time is quite different and a slight oscillation appears but specifications are fulfilled. These results confirm that the simplified aircraft and control model is sufficiently representative of a real aircraft behaviour.

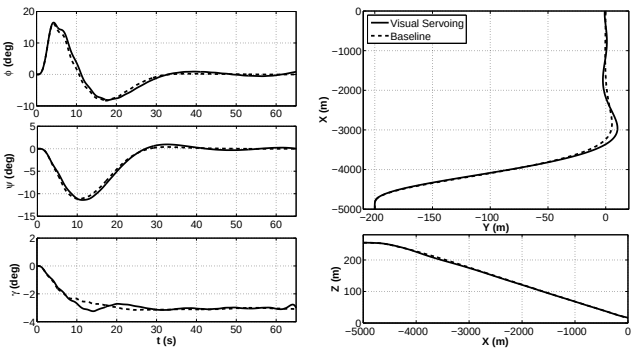

Fig. 16. Simulation on a nonlinear simulator

The simplified camera and image processing model have also been validated by using a viewer and real image processing algorithms. Even if image processing produces noisy values of visual features, it confirms that the simplified model is representative of real image processing behaviour.

5. CONCLUSION AND FUTURE PERSPECTIVES

This paper presented a benchmark of different IBVS solutions to perform automatic aircraft landings. After applying previously proposed strategies to an AIRBUS benchmark model and analyzing the performance against the baseline solution, a new set of visual features was proposed to cope with coupling and non linear effects and tried to make control design as linear as possible. This new strategy seems to fulfill our specifications and matches the baseline guidance laws performance when validated on a full non-linear simulator. However, the distance to the runway still has an influence on the guidance law performances. Our future work will focus more deeply on non-linear effects analysis and on non-linear controller design to cope with lateral/longitudinal coupling in order to get a bigger "region of attraction" and also to take into account wind perturbations.

REFERENCES

Azinheira, J.R. and Rives, P. (2008). Image-Based Visual Servoing for Vanishing Features and Ground Lines Tracking: Application to a UAV Automatic Landing. *International Journal of Optomechatronics*, 2, 275–295.

Bourquardez, O. and Chaumette, F. (2007a). Visual servoing of an airplane for alignment with respect to a runway. In *IEEE Int. Conf. on Robotics and Automation, ICRA'07*, 1330–1335. Rome, Italy.

Bourquardez, O. and Chaumette, F. (2007b). Visual servoing of an airplane for auto-landing. In *IEEE/RSJ Int. Conf. on Intelligent Robots and Systems, IROS'07*, 1314–1319. San Diego, CA.

Coutard, L., Chaumette, F., and Pflimlin, J.M. (2011). Automatic landing on aircraft carrier by visual servoing. In *IEEE/RSJ Int. Conf. on Intelligent Robots and Systems, IROS'11*, 2843–2848. San Francisco, USA.

Goncalves, T., Azinheira, J., and Rives, P. (2010). Homography-based visual servoing of an aircraft for automatic approach and landing. In *IEEE International Conference on Robotics and Automation*. Lisbon, Portugal.

Hughes, F.J. (October 2012). Wide-area augmentation system performance analysis report report #42 reporting period: July 1 to september 30, 2012. Technical report, NSTB/WAAS T&E Team.

Le Bras, F., Hamel, T., Barat, C., and Mahony, R. (2009). Nonlinear image-based visual servo controller for automatic landing guidance of a fixed-wing aircraft. In *European Control Conference*, 1836–1841.

Magni, J. (2002). *Robust Modal Control with a Toolbox for use with Matlab*. Kluwer Academics/Plenum publishers.

Silveira, G., Azinheira, J., Rives, P., and Bueno, S. (2003). Line following visual servoing for aerial robots combined with complementary sensors. In *IEEE International Conference on Advanced Robotics*. Coimbra, Portugal.